buildings

MDPI

Article

Experimental and Numerical Investigations of Laced Built-Up Lightweight Concrete Encased Columns Subjected to Cyclic Axial Load

Nagarajan Divyah [1], Ramaiah Prakash [2,*], Sundaresan Srividhya [3], Siva Avudaiappan [4,5,6,*], Pablo Guindos [5], Nelson Maureira Carsalade [7], Krishna Prakash Arunachalam [8], Ehsan Noroozinejad Farsangi [9] and Ángel Roco-Videla [10,*]

1 Department of Civil Engineering, PSG Institute of Technology and Applied Research, Coimbatore 641062, India
2 Department of Civil Engineering, Government College of Engineering, Tirunelveli 627007, India
3 Department of Civil Engineering, Varuvan Vadivelan Institute of Technology, Dharmapuri 636703, India
4 Departamento de Ingeniería Civil, Universidad de Concepción, Concepción 4070386, Chile
5 Centro Nacional de Excelencia para la Industria de la Madera (CENAMAD), Pontificia Universidad Católica de Chile, Av. Vicuña Mackenna 4860, Santiago 8330024, Chile
6 Department of Physiology, Saveetha Dental College and Hospitals, SIMATS, Chennai 600077, India
7 Departamento de Ingeniería Civil, Facultad de Ingeniería, Universidad Católica de la Santísima Concepción, Concepción 4090541, Chile
8 Department of Civil Engineering, University College of Engineering Nagercoil, Anna University, Nagercoil 629004, India; krishnaprakash3191@gmail.com
9 Department of Civil Engineering, The University of British Columbia (UBC), Vancouver, BC V6T 1Z4, Canada
10 Facultad de Salud y Ciencias Sociales, Universidad de las Américas, Providencias, Santiago 7500975, Chile
* Correspondence: rprakash024@gmail.com (R.P.); savudaiappan@udec.cl (S.A.); aroco@udla.cl (Á.R.-V.)

check for updates

Citation: Divyah, N.; Prakash, R.; Srividhya, S.; Avudaiappan, S.; Guindos, P.; Carsalade, N.M.; Arunachalam, K.P.; Noroozinejad Farsangi, E.; Roco-Videla, Á. Experimental and Numerical Investigations of Laced Built-Up Lightweight Concrete Encased Columns Subjected to Cyclic Axial Load. *Buildings* **2023**, *13*, 1444. https://doi.org/10.3390/buildings13061444

Academic Editor: Petr Mynarčík

Received: 23 April 2023
Revised: 14 May 2023
Accepted: 29 May 2023
Published: 31 May 2023

Abstract: The steel-concrete composite column comprises a steel core and surrounding concrete. The purpose of the system is to provide analysis and design techniques for a newly invented class of laced steel-concrete composite short columns for cyclic axial loads. To minimize the increasing density issues associated with nominal strength concrete and in consideration of the depletion of natural resources required to produce concrete, factory-obtained lightweight sintered fly ash aggregates with and without basalt fiber are employed. The normal-weight concrete containing basalt fiber is shown to be more ductile than any other column. The axial deformation of columns LNA and LSA at failure was found to be 3.5 mm, whereas columns LNAF and LSAF reached an axial shortening of 4.5 mm at failure. The column LSAF was found to have 5.3% more energy absorption than the LSA and 11.5% less than the column LNAF. It was observed that the rigidity of these fabricated components had been enhanced. It was found that the section configuration with a lacing system had improved confinement effects and ductility. Comparing the finite element analysis to the experimental data revealed a strong connection with numerical modeling, with a variance of around 8.77%.

Keywords: laced built-up column; basalt fiber; lightweight concrete; strain behavior; finite element analysis; deformation

1. Introduction

The use of steel-concrete composite members is essential to preventing rust and fire on reinforcing steel. The encased concrete has a significant impact on the strength, serviceability, and durability of the structural element. The use of structural members as reinforcement was not well pronounced in the early 1950s. The continuous efforts of researchers have emphasized the benefits of composite columns by encasing the steel profile [1]. Emperger [2] was the first to conduct tests on built-up columns. Concentric loading was applied to the composite columns, and the test results were presented. Burr [3] conducted experiments on enclosed latticed steel-concrete-encased columns and concluded

that the encasement of concrete gave a significant boost in strength. Yee et al. [4] offered design expressions for a novel style of building in which steel channels were connected with battens and concrete was filled. Weng & Yen [5] studied the design of concrete-encased composite columns and found differences in the AISC and ACI techniques. Eom et al. [6] studied the encased composite columns with bolted end-plate splicing of steel angles. A thick end plate is suggested in accordance with the yield line hypothesis, and it is expected that when force is applied, the tensile strength of the connection will diminish. The yielding and failure of the connection do not result in the brittle failure of the entire column. Concrete-encased steel (CES) composite short columns exposed to pure monotonic compression were explored by Lai et al. [7] for their axial compressive performance. By lowering the spacing between the ties, the column's ultimate load capacity can be increased, although failure is brittle with a sudden drop in ultimate load. The inclusion of steel fibers significantly reduced concrete spalling and increased the loading capacity. To prevent early concrete spalling and brittle failure in CES stub columns, Khan et al. [8] examined the behavior of a special type of engineered cementitious composite (ECC). The ECC encasing enhanced the failure pattern, toughness, and ductility of the columns under compression. Strain analysis was utilized to identify strain patterns and physical damage in materials. In recent times, built-up laced columns have found their application in bridges and tall buildings as lightweight steel structures. Most of the codal provisions allow these columns to be designed only for axial loads [9,10]. Rigorous research is in progress focusing on the seismic behavior of these columns, the effect of shear on the axial compression loading of these columns, and the analysis of buckling behavior [11]. When an earthquake causes a lateral load on a built-up column, it may not behave as expected. Therefore, to meet the requirements of vibration and earthquake loading in addition to fire protection and protection against corrosion, the encased concrete is made of higher quality. The research on the behavior of composite columns and the revision of current design guidelines are motivated by advancements linked to the usage of high-performance concrete and seismic effects [12,13]. Giménez et al. [14] performed laboratory experiments on steel gage-strengthened reinforced concrete columns. With this increase in the number of stirrups, the ultimate load of the strengthened column improved due to the confinement effect. Hosseini & Jafari [15] constructed a column with two numbers of IPE100 longitudinal chords and plates instead of lacing and tested it for axial and cyclic loads. The ductility, strength, and stiffness of the built-up columns were significantly affected by the axial load. The test findings suggested that the laced columns might be used in moderately earthquake-prone regions. The seismic behavior of built-up, laced steel brace members for quasi-static testing was investigated in an experiment by Lee and Bruneau [16]. The performance of built-up cold-formed steel (CFS) angle section columns with a single lacing system under monotonic axial loads was studied by Dar et al. [17].

Wasserman and Bentur [18] explored the interactions between the matrix in Portland cement concretes and sintered fly ash lightweight particles to resolve difficulties that influence concrete strength other than aggregate strength. Most of the time, it was determined that variations in aggregate strength could not be explained by changes in concrete strength. Densification of the interfacial transition zone causes the enhancement of strength. It should be considered when designing a lightweight aggregate with optimal characteristics. Wasserman and Bentur [19] used some treatments, such as heat and polymer, to modify the sintered fly ash lightweight aggregate structure, resulting in aggregates with varying strengths, absorption, and pozzolanic activity. It was shown that the strength of the aggregates alone could not account for the strength of the concrete, but the pozzolanic phenomenon may have an impact on the development of strength. According to Jayanthi et al. [20], concrete is composed of coarse aggregate and cement mortar, and these parameters are responsible for its strength. In lightweight aggregate concrete, when the elastic modulus of the aggregate and mortar is equivalent, a critical scenario occurs during the strength increase stage [21]. According to a method suggested by Sirikul and Wijeywickrema [22], the tensile strength of fly ash aggregate increased according to the

equivalent CaO concentration of the raw materials employed in its production. The effects of synthetic and metallic fibers on sintered fly ash lightweight aggregate and high-strength concrete were studied by Sheebha et al. [23]. Other mechanical properties were unaffected by the introduction of polypropylene fiber. The stress-strain curve and the modulus of elasticity were both slightly impacted by steel fiber. A considerable enhancement of the compressive strength and toughness was found. It revealed a considerable increase in ductility when steel fiber reinforcing was utilized. Haque et al. [24] tested two lightweight aggregate concretes that were water-cured continuously for seven days. It was subsequently subjected to a hot, humid seashore environment with airborne salts. The results showed that compressive strength was less sensitive to the tested curing regimes. Both chloride and sulfate penetration were determined to be below acceptable levels after a year of exposure.

Rohman and Aji [25] experimented with the use of lightweight fly ash aggregate in polymer concrete. It was revealed that the tensile strength/compressive strength ratio was notably higher than that of traditional cement concrete. Guneyisi et al. [26] examined segregation in polymer concrete with sintered fly ash and crushed granite aggregates. There is no segregation at the coarse aggregate when sintered fly ash aggregate is used. Nonetheless, the granite aggregate particles sink to the bottom, resulting in visible segregation in the mix. Kayali [27] demonstrated that concrete constructed using sintered fly ash aggregates is 22% lighter, 20% stronger, and 33% less susceptible to drying shrinkage than conventional concrete. With the use of these aggregates, the amount of cement needed to achieve the same strength can be lowered by up to 20%. The low self-weight may reduce the cost of transporting precast concrete while allowing for slimmer and more expansive structures. The test findings indicated that the newly developed concrete is lightweight, porous, strong, and has a great potential for durability. This lightweight aggregate concrete is more than 21% lighter than aggregate concrete composed of granite and dacite. Kockal and Ozturan [28] elucidated that the LWC has a comparable ratio of tensile to compressive strength to normal-weight concrete. Durability requirements for freezing and thawing were satisfied by the durability factor. The strength properties of cold-bonded and sintered fly ash aggregates were carefully compared by Gomathi and Sivakumar [29]. The concept of aggregate packing was utilized to develop concrete mixtures of mortar and fly ash aggregate in varied combinations. After curing in hot water, the sintered fly ash aggregate concrete mix containing it showed 62% more compressive strength. Sintered fly ash aggregates have a higher water absorption rate and a specific gravity that is 16 to 46% lower than traditional aggregates [30]. Sintered fly ash aggregate concrete has compressive strengths varying between 27 and 74 Mpa and a density varying between 1651 and 2017 kg/m^3.

The basalt fiber increases ductility and energy absorption capacity [31]. The steel core within the encased concrete consists of a laced, cold-formed, built-up steel member. The elements fabricated were short columns with axial cyclic loading. These columns are developed for use in vibration floors such as dance floors and floors with machine foundations.

The effects of basalt fiber length and volume (BF) on the hardened properties of fiber-reinforced concrete were investigated by Jiang et al. [32]. Except for compressive strength, the results indicated that the mechanical properties were greatly enhanced. Qin et al. [33] studied the influence of basalt fibers of varying fractions in a magnesium phosphate cement matrix and found that flexural strength, split tensile strength, and fracture toughness increased significantly with basalt fiber addition. Kharun et al. [34] experimented with the basalt fiber high-strength concrete and found that the basalt fibers significantly decreased the compressive strength while increasing the tensile strength. Galishnikova et al. [35] determined that the ductility of basalt fiber-reinforced concrete was enhanced by the fiber fraction, fiber length, and diameter.

To explore the behavior of concrete-encased, concrete-filled steel tube (CFST) columns subjected to axial load, Han & Yufeng [36] developed a finite element approach and proposed easier formulas for the prediction of the ultimate strength of the column. In a study, Zhang et al. [37] examined the behavior of an equal-leg angle steel composite

column for its ultimate load and ductility. Balaz et al. [38] examined a previously validated nonlinear numerical model to simulate the behavior and predict the ultimate load of coupled laced columns using the finite element method. The effect of lacing patterns, load eccentricity, and column length on the capacity of built-up beam columns is investigated in depth.

In earlier experiments, composite columns with conventional concrete of nominal strength and high strength as encasings and with regular profile steel were examined. The issue with utilizing concrete with nominal strength is that it has an increased density and the resources needed to produce it are rare, but high-strength concrete has a problem with brittle failure. To avoid fragile failure, steel fibers are being employed. The angle sections placed at the corners and connected by lacings enhance the capacity of the column and its structural performance. For high-strength concrete, additional experimental and numerical research is necessary to prevent brittle fracture. To employ lightweight particles as either high-strength or nominal-strength concrete, however, limited research has been done. There is no conclusive research on the failure modes or structural behavior of this type of concrete when used as encasing. In addition, the substitution of basalt fiber for steel fiber is not prominent. Therefore, this research is deemed appropriate to create a unique and required research document that incorporates the structural performance and application of lightweight laced, built-up concrete-encased composite columns. The research idea based on the effective use of locally accessible resources could place the laced lightweight concrete-encased composite columns far ahead of their use in real projects as well.

2. Materials and Methods

2.1. Proposed System

Four cold-formed angle sections were positioned longitudinally on each of the four corners of the laced, built-up composite short column. These sections were connected by lacings that were connected at a 45-degree angle in all directions. The columns were designed as per EN 1994-1-1 and Eurocode 4. The cold-formed angle sections were manufactured by pressing cold-formed steel plates under pressure. This steel core functions as reinforcement and is individually encased in NWC and LWC, with or without basalt fiber. The concrete-encased composite column is composed of both hardened concrete and a steel core.

Four test specimens were cast utilizing laced steel arrangements and concrete encasement types. The slenderness ratio of the columns was designed such that they can be classified as short columns (700 100 100 mm). For the investigation, laced-up prefabricated steel shapes of modest size and medium-strength 30 MPa concrete with a 20 mm cover were selected. The gradation of materials was chosen to permit a good concrete encasement around the steel section, which is more suitable for small-scale models. The lightweight encased concrete is composed of artificially sintered fly ash and lightweight aggregates. The lightweight sintered fly ash concrete was chosen for the study to reduce the dead load on the column. It leads to a reduction in the overall dead load on structures, a reduction in element size with increased load-carrying capacity, and enhanced performance. The size of the sintered fly ash aggregates used was 12 mm. Figure 1 shows the materials utilized for making concrete.

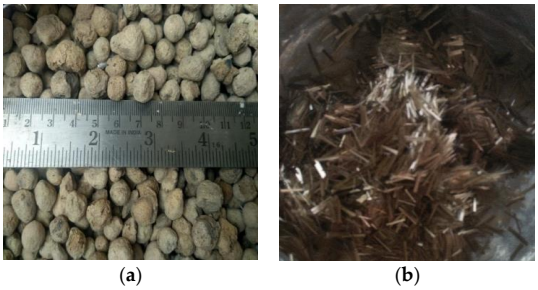

(**a**) (**b**)

Figure 1. Details of the materials used. (**a**) Sintered fly ash aggregate. (**b**) Basalt Fibre.

2.2. Experimental Investigation

Table 1 provides the engineering properties of the concrete used to make up the encasement of the column specimen. For making the angle sections, cold-formed sheets of thickness 1.6 mm and yield strength 260.34 MPa, confirming Indian standards [39], were used. The yield strength of the steel sheet was 260.34 MPa, found using a coupon test.

Table 1. Engineering properties of the column.

Sl No.	Column ID	Type of Concrete	f_{ck} (MPa)	E (GPa)	Density (kg/m^3)
1	LNA	Normal weight concrete	38.04	305	2567
2	LNAF	Fiber-reinforced normal-weight aggregate concrete	40.56	353	2671
3	LSA	Lightweight concrete	38.62	223	2113
4	LSAF	Fiber-reinforced lightweight aggregate concrete	41.88	299	2220

A steel capping plate was made and fastened at the top and bottom for stability and to allow axial loading. To prevent local crushing at the point of load application and premature column collapse, each composite column was covered with 100 mm of high-strength GFRP sheets at the top and bottom, as shown in Figure 2. Figure 3 depicts the built-in reinforcement of the column.

Figure 2. Columns prepared for testing.

Figure 3. Reinforcement skeleton with Laced Configuration.

2.3. Experimental Set-Up

The columns were tested for axial cyclic loading in a loading frame using the following arrangements: The test setup for the specimens is shown in Figure 4. End steel plates were

utilized at the top and bottom of the specimen to apply the load. The specimen's verticality was preserved with due diligence. An LVDT was fastened vertically to the column end plate to measure the axial shortening. The linear and lateral strains were determined by installing strain gauges at the center point that were parallel and perpendicular to the column axis and connecting them to a 10-channel strain indicator. The load cell, which is placed over the column, is equipped with a digital load indication. The weight is applied using a hydraulic jack with a 50 T capacity that is driven by a battery pack. The test column is firmly fixed using the steel capping plates at the top and bottom. High-strength plaster and high-strength GFRP sheets are used to level the column's top and bottom faces, ensuring even load distribution and preventing premature column crushing. For each load increment, the deformation and strain values are listed.

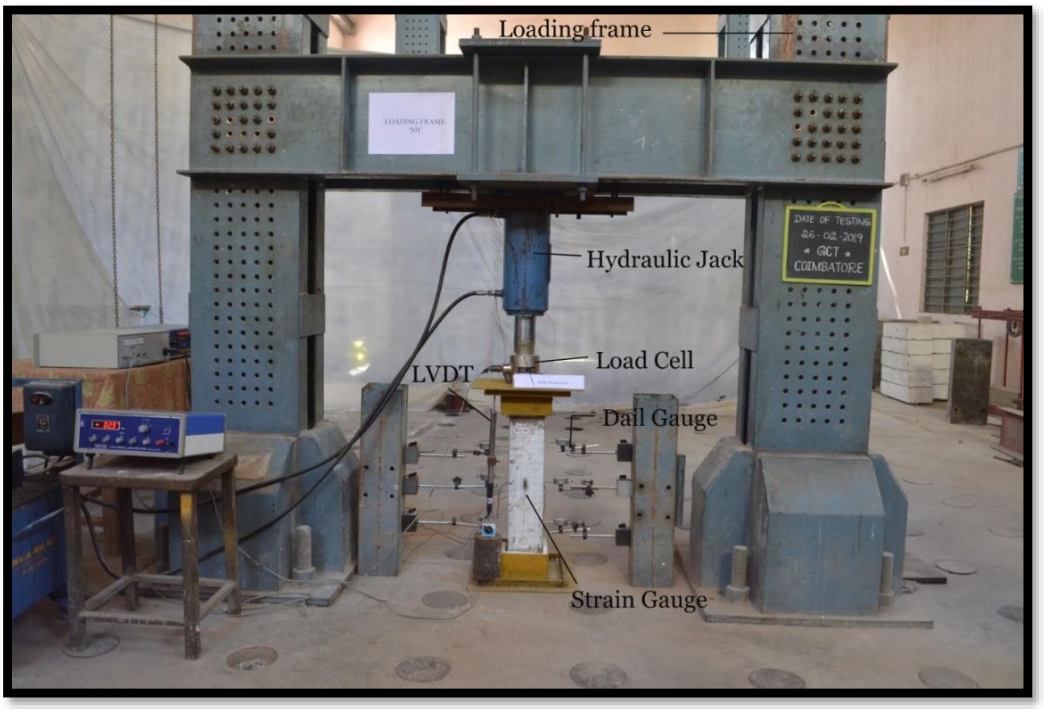

Figure 4. Schematic test setup.

2.4. Finite Element Analysis

The structural reaction of the previously disclosed concrete-encased lace-built-up columns was numerically simulated using the general-purpose FE software ANSYS 16.1. The generated models were validated against all individual experimental results. In this analysis, several material models for concrete, steel, and GFRP sheets were used, and interaction between these elements was developed using interaction models. For the column, nonlinear three-dimensional finite element models that take into account the geometry, material, loading, and boundary conditions were created. The model is confined by displacement boundary conditions to yield a unique solution. Boundary conditions are imposed on the faces of the model to ensure that it behaves similarly to the experimental column.

The Drucker-Prager plasticity model was adopted for the non-linear material modeling of the column. The three stages of the column's finite element modeling in ANSYS are detailed below, and Table 2 displays the input properties of the materials employed.

- Element type selection
- Material properties assigning
- Geometry modeling and meshing

Table 2. Details of Element and material properties.

S. No	Name	Material	ANSYS Element
1.	Concrete	NA, NAF, SA, SAF	Solid 185
2.	Steel Angle section (12 × 12 × 1.6 mm)	CFS	BEAM 188
3.	End Wrapping	GFRP	Shell 181

2.4.1. ANSYS Geometric Model

To generate the finite element model in ANSYS WORKBENCH 16.1, the FEA study involved modeling a concrete column with dimensions and qualities matching those of the column examined experimentally. The reinforcement (1D model) and concrete (3D model) models were made using the ANSYS DESIGN MODELER environment.

2.4.2. Finite Element Meshing

Following model generation, the model is separated into many finite elements by meshing. The choice of mesh density is a crucial stage in finite element modeling; hence, a finer mesh was chosen to model the column. The experimental analytical details were used to develop the wireframe structures for the column's steel reinforcement detailing. Figure 5 depicts a visual illustration of the meshed column.

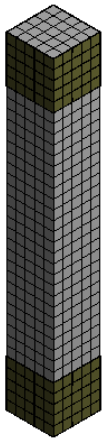

Figure 5. Column before loading (mesh modeling).

2.4.3. Application of Loads and Boundary Condition

To constrain the model and yield a single solution, displacement boundary constraints were applied at the faces to guarantee that the created model behaves similarly to the experimental column. The boundary condition was simulated with columns fixed at both ends, as shown in Figure 6.

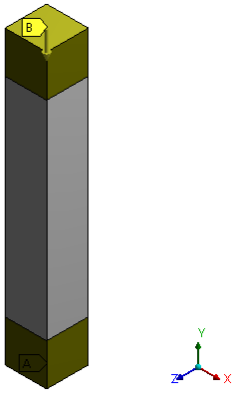

Figure 6. Loading condition of the column.

3. Results and Discussion

3.1. Axial Shortening

Experimentally, the axial shortening of the specimens was determined by vertically mounting an LVDT beneath the steel plate covering the column specimen (Figure 7). The axial deformation of columns LNA and LSA at failure was found to be 3.5 mm, whereas columns LNAF and LSAF reached an axial shortening of 4.5 mm at failure. After the ultimate load was reached, with further increments in loads, the column LNA sustained two more cycles, whereas other columns could sustain one cycle after the ultimate load. The last cycle was more pronounced with large deformation than the other cycles, even at small load increment levels, and finally failed with a rhombic-like load-deformation curve [15,40,41].

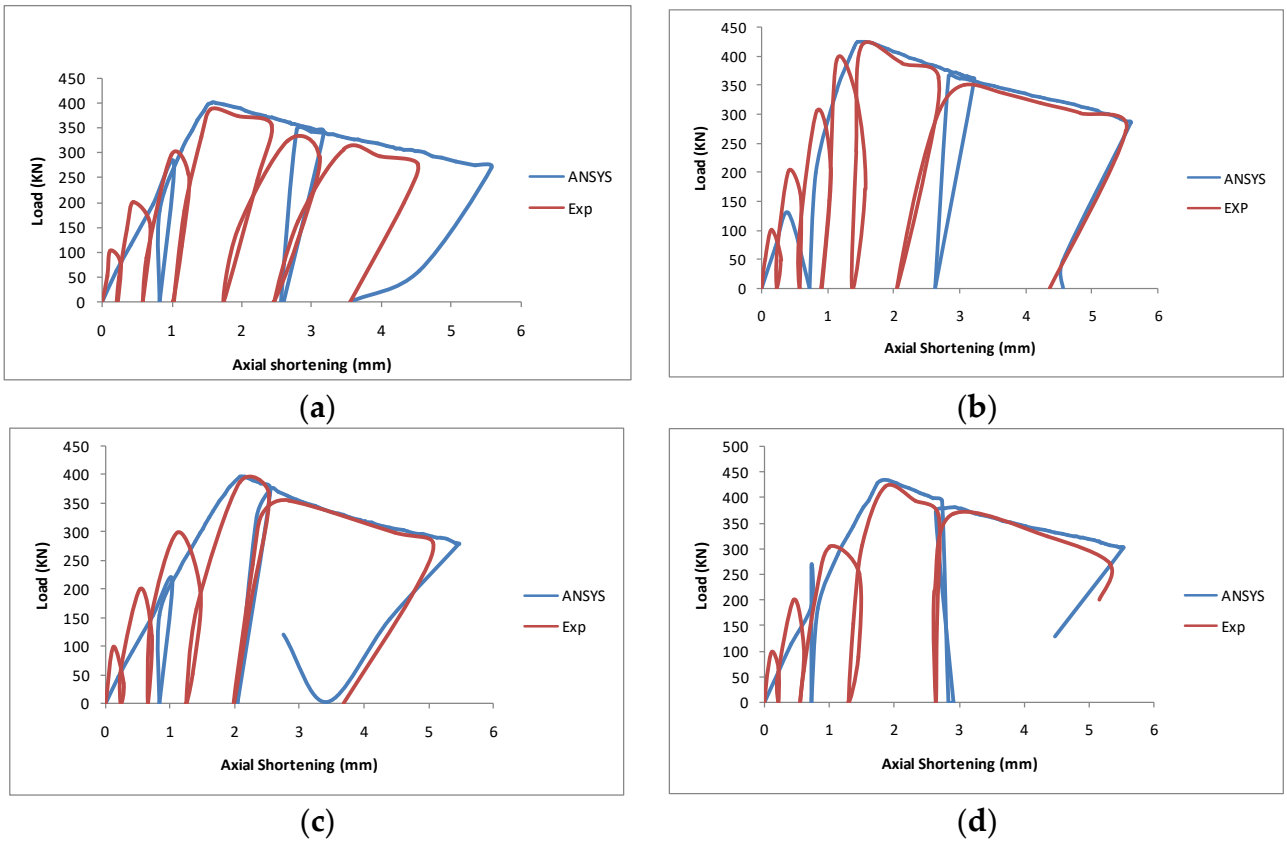

Figure 7. Axial load deformation patterns. (**a**) LNA—Normal-weight Column. (**b**) LNAF—Fibre Reinforced Normal-weight Column. (**c**) LSA—Lightweight Column. (**d**) LSAF—Fibre Reinforced Lightweight Column.

There was no significant axial deformation noted until the first three cycles. The lateral deformation was prominent only when the major crack appeared on the specimen. From Figure 8, it is evident that the specimens started to fail soon after the ultimate load with large deformations when compared to the previous cycles. The deformation of the specimen LNAF at the ultimate load is 0.74 times higher than that of LNA, whereas the specimens LNA and LSAF attained almost the same deformations at the ultimate load. The specimen LSA deformed 3.83 times more than the specimen LNA, and the deformation of the specimen LSAF was 0.4 times less than that of the LNAF.

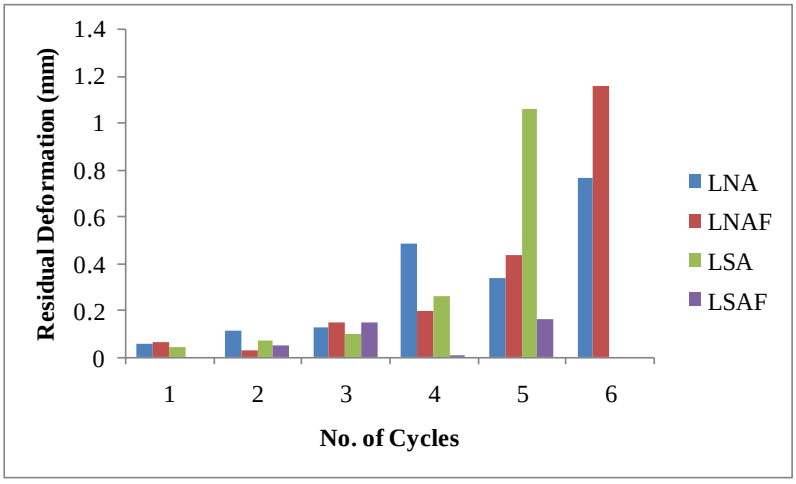

Figure 8. Residual Deformation.

3.2. Cracking Displacement

When significant cracks first appeared, the displacements were measured. The concrete started to fail with the onset of the first major crack. The columns LNA and LSAF were pronounced with a major crack at the initiation loading phase of the 4th cycle, whereas the column LNAF was detected with a major crack at the commencement of the 5th cycle. The column LSA was found with a major crack at the 3rd cycle itself. The axial shortening of all these columns was the same at the cracking load. However, the lateral deformation of the column LNA is 0.6 times higher than that of the column LNAF, whereas the lateral deformation at the onset of a major crack for the column LSA is 1.5 times greater than that of the column LNA. The columns LNAF and LSAF had similar lateral deformation on the first crack load, which indicates the role of fiber in arresting the deformations when added to the concrete matrix. Table 3 shows the load and deformation values at the first crack and ultimate stages.

Table 3. Load-Deformation at first crack and ultimate stage.

Column ID	First Crack		Ultimate	
	Load (kN)	Deformation (mm)	Load (kN)	Deformation (mm)
LNA	295	0.993	386.0035	1.559
LNAF	306	0.84	417.238	1.507
LSA	298	1.11	387.562	2.068
LSAF	303	0.998	421.345	1.864

3.3. Ultimate Displacement

The ultimate deformation under each cycle was noted, and it was obvious that the columns LNA and LSA were found to have higher deformation when compared to LNAF and LSAF. With the increase in load cycles, the deformation of the column LNAF gradually decreased, and overall it sustained the least ultimate deformation when compared to other columns. The ultimate deformation of the column LSA was found to be greater when compared to other columns under all load cycles.

3.4. Residual Deformation

The residual deformation is presented in Figure 8. The columns had very little residual deformation at the initial cycles of load increment and decrement. However, after the 3rd cycle, the column LNA had a sudden increase in residual deformation that decreased with a further increase in load cycles. The column LSA was found to have residual deformation with each increment in load cycles and lasted with a significant residual deformation only at the last cycle. The column LSAF was found to have the least residual deformation at

all cycles. At the end of load cycles, the columns LNAF and LSAF are pronounced with more residual deformations. The effect of residual deformation comes into play with more resistance of the concrete to cracking and with better reinforcement.

3.5. Energy Absorption Capacity

Figure 9 depicts the energy absorption of columns. The energy absorption capacity of the column LNA increased up to the 4th cycle and then suddenly decreased at the 5th cycle, after which it increased at the last cycle, whereas the other columns had increased energy absorption with the progression of load cycles. This increase is due to the confining effects of the laced composite structure, together with the effect of concrete. The cumulative energy absorption of column LNAF is 25% higher than that of column LNA, whereas column LSA has 5% more energy absorption than column LNA. Column LSAF was found to have 5.3% more energy absorption than LSA and 11.5% less than column LNAF.

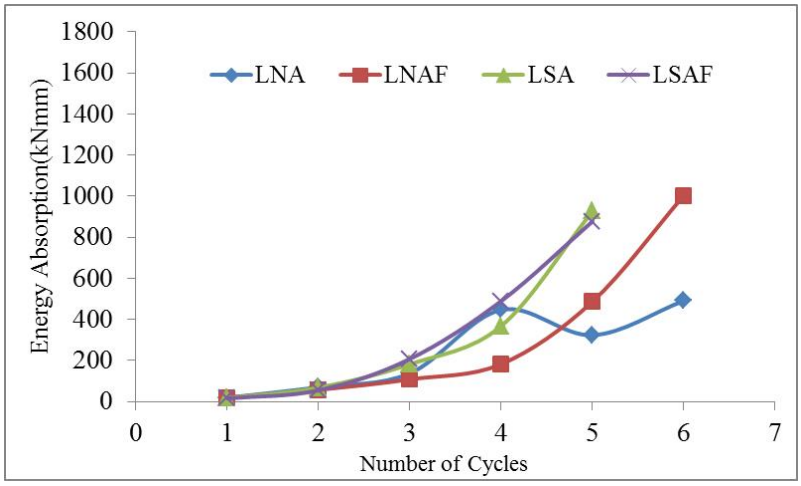

Figure 9. Energy absorption.

3.6. Ductility

Based on FEMA356, an envelope curve was traced in Figure 10 to classify the ductility of the specimen. The ductility factor is calculated by considering the yield load at 75% of the ultimate load. Column LNAF showed a 2% higher ductility factor than column LNA, whereas LSA has a 13% lower ductility than column LNA. Column LSAF had 8% more ductility than LSA and 19% lower ductility than column LNAF. The ability of the columns to withstand large deformations without significant deformations was well pronounced by the column LNAF.

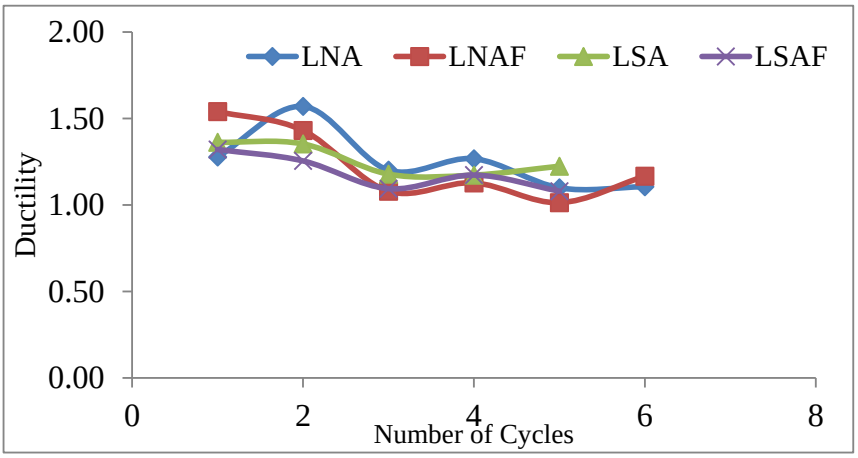

Figure 10. Ductility.

3.7. Stiffness Degradation

The stiffness degradation of columns of test series III under each cycle is shown in Figure 11. The stiffness behavior of the LNA column was high at the first cycle, and it started to decrease at a steady rate at each successive increment in cyclic loading. The LNAF column had increasing stiffness up to the 5th cycle, and it decreased at the 6th cycle. In the 5th cycle, there was an enormous increase in stiffness when compared with other cycles. The LSA and LSAF columns had decreasing stiffness at each successive cyclic load increment.

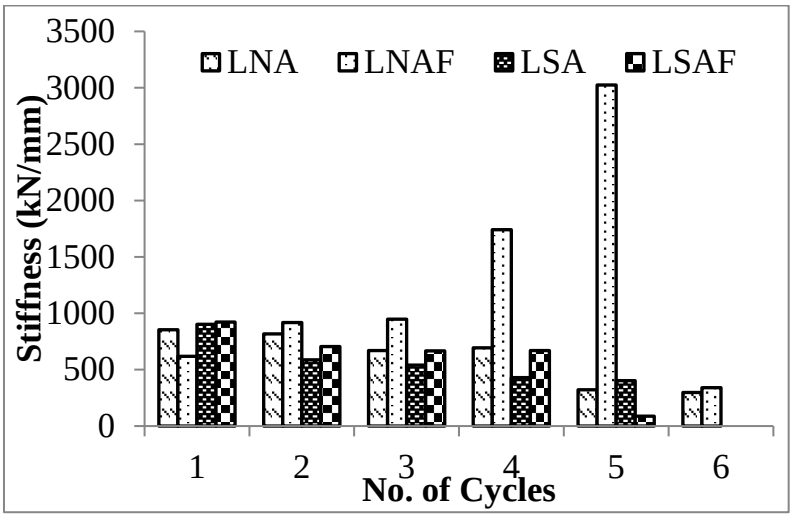

Figure 11. Stiffness Degradation of Test Series III under each cycle.

3.8. Observed Behaviour and Failure Mode

The columns were fixed at their positions and loaded with load increments and load reversals. Concrete compression or crushing predominated in the failure of the columns [42]. However, even after the appearance of a major crack, the column continued to withstand more loads. The role of the laced steel core plays a critical role here. Figure 12 shows the failure of the columns. The LNA and LSA columns were found to have vertical cracks along one corner. The LNAF column has a shear crack along one face of the column. The column LSAF was found to have some major cracks just below the GFRP lining. Almost all columns were found to have a minor crack that appeared at the end of the load increment in the second cycle. The first major crack appeared in the column LNA in the 4th cycle following a minor crack that developed at the bottom, but at the initiation of the 5th cycle, a major vertical crack suddenly started to appear at one side of the specimen just below the GFRP wrapping. It propagated at a faster rate, and the ultimate load was reached with subsequent load increments in the same cycle. Considering column LNAF, minor cracks were found surrounding the GFRP wrapping in all four corners right from the initiation of the 3rd cycle. Similar to column LNA, a minor crack suddenly appeared at the initiation of the 5th cycle, and it transformed into a shear crack even before the ultimate load. In column LSA, the corners of the column just below the GFRP wrapping started to chip off with the initiation of the 3rd cycle, and a sudden vertical crack developed at the top portion of the column at the load increment phase of the 4th cycle. The specimen reached the ultimate load, after which the crack propagated, resulting in final failure. The column LSAF failed with a large number of cracks, both major and minor, along with the four faces of the specimen. As with the column LSA, the column LSAF also reached its maximum capacity at the 4th cycle, and failure reached the 5th cycle. The only difference is that more minor cracks were found along the top face of the specimen LSAF.

(**a**) (**b**) (**c**) (**d**)

Figure 12. Typical failure modes of the column. (**a**) Normal weight Column. (**b**) Fibre Reinforced NWC Column. (**c**) Lightweight Column. (**d**) Fibre Reinforced LWC Column.

3.9. Convergence of Experimental and Finite Element Modeling

3.9.1. Strain Behavior

Finite element analysis is a numerical method of investigation used to solve problems in engineering that require unique analysis [43]. It is a powerful computational technique for solving structural problems with many variables [44]. This method of analysis is carried out using the solid modeling and analysis software ANSYS. Observing the strain behavior of the column at failure obtained from finite element analysis, as depicted in Figure 13, reveals that the columns LSA and LSAF were stressed up to 0.0025, whereas the columns LNA and LNAF were strained at 0.002.

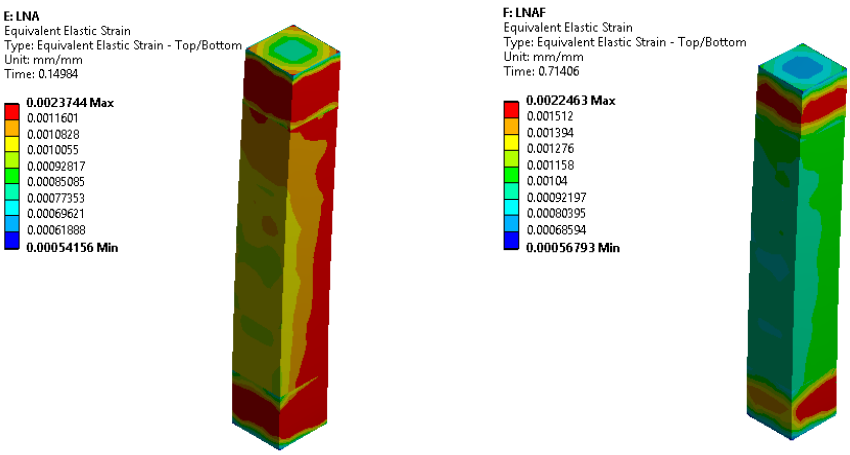

(**a**) (**b**)

Figure 13. *Cont.*

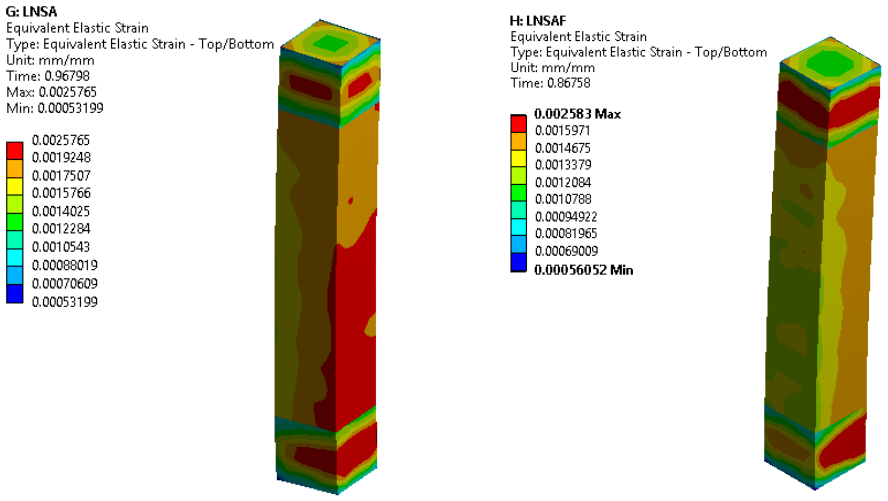

(**c**) (**d**)

Figure 13. Observed strain in Columns from FEA. (**a**) Normal weight Column. (**b**) Fibre Reinforced Normal weight Column. (**c**) Lightweight Column. (**d**) Fibre Reinforced Lightweight Column.

The red contour represents the plastic hinge zone, which corresponds to the locations where the failure occurred in the experimental columns. The FEA-obtained plot demonstrates that the largest crack emerged in locations where plastic hinges had formed [45]. At the ultimate load, the columns LNA and LNAF are observed to have a strain value of 0.001, but the columns LSA and LSAF are observed to have a strain value of 0.002.

3.9.2. Deformation

The experimentally determined load deformations were then compared to the FEA-determined load deformations. Axial and lateral deformations were respectively 0.64 and 5.96%, while the difference in the column LNA's maximum load-bearing capacity was 3.77%. The final load-carrying capacity of the LNAF column varied by 2.01%, with axial and lateral deformations of 3.98 and 7.48%, respectively. The capacity and axial deformation of the LSA column varied by 2.48 and 0.63%, respectively, but the lateral deformation varied by 6.84 percent. The maximum capacity of the LSAF column varied by 3.08%, whereas the axial and lateral deformations varied by 2.55% and 1.5%, respectively. Table 4 displays the discrepancy between the experiment and ANSYS based on the observed data. The results of FEA are found to be better than the experimental results, and both the experimental results and the FEA results are well correlated [46]. The largest forecast error is 8.77%.

Table 4. Difference in observed results obtained from the experiment and ANSYS.

Column ID	Experiment			ANSYS		
	Load (kN)	Axial Deformation (mm)	Lateral Deformation (mm)	Load (kN)	Axial Deformation (mm)	Lateral Deformation (mm)
LNA	386.00	1.559	0.302	400.56	1.569	0.32
LNAF	417.24	1.507	0.527	425.64	1.567	0.566
LSA	387.56	2.068	1.46	397.16	2.081	1.559
LSAF	421.34	1.864	0.303	434.31	1.91	0.308

4. Conclusions

The analysis of lightweight, laced, reinforced concrete columns subjected to cyclic axial loads was performed. The following conclusions were obtained, emphasizing the uniqueness and utility of the study's findings from a scientific perspective:

- The axial deformation of columns LNA and LSA at failure was found to be 3.5 mm, whereas columns LNAF and LSAF reached an axial shortening of 4.5 mm at failure.

- There was no significant lateral deformation noted until the first three cycles. At the failure load, the lateral deformations of columns reinforced with basalt fiber were found to be significantly lower due to the fiber bridging phenomenon within the concrete matrix.
- The columns LNA and LSAF were pronounced with a major crack at the initiation loading phase of the 4th cycle, whereas the column LNAF was detected with a major crack at the commencement of the 5th cycle. The column LSA was found with a major crack at the 3rd cycle itself.
- The ultimate deformation of the column LNA was found to be greater when compared to other columns under all load cycles.
- At the end of load cycles, the columns LSA and LSAF are pronounced with more residual deformations.
- Column LSAF was found to have 5.3% more energy absorption than LSA and 11.5% less than column LNAF.
- Although the column LNAF was found to have a shear crack along the length of the specimen, it was found to be more ductile with more energy absorption than other columns.
- On tracing a failure envelope over the load-deformation curve, the columns were found to be well confined with better load-deformation characteristics.
- The ability of the columns to withstand large deformations without significant deformations is well pronounced by the column LNAF.
- When compared to the experimental results, the predictions based on finite elements demonstrated that the failure had occurred precisely where plastic hinges had been formed.
- The advantage of lightweight concrete combined with a better laced built-up section creates a unique composite system that performs well in vibration loading as normal-weight concrete.
- It is recommended to optimize the spacing between the steel angles so that there will be changes in the confinement effects and structural behavior. Also, the volume of basalt fibers can be increased for better performance in LSAF columns compared to LNAF columns.

Author Contributions: Conceptualization, N.D., R.P., S.S., S.A., P.G., N.M.C., K.P.A., E.N.F. and Á.R.-V.; Methodology, N.D., R.P., S.S., S.A., N.M.C. and K.P.A.; Software, N.D., R.P., S.S., S.A., P.G., N.M.C., K.P.A. and Á.R.-V.; Validation, N.D., R.P., S.S., S.A., N.M.C., K.P.A., E.N.F. and Á.R.-V.; Formal analysis, N.D., R.P., S.A., P.G., N.M.C. and K.P.A.; Investigation, N.D., R.P., S.S., S.A., P.G., N.M.C., K.P.A. and E.N.F.; Resources, R.P., S.A., P.G., N.M.C. and K.P.A.; Data curation, S.S., S.A., N.M.C. and K.P.A.; Writing—original draft, N.D., R.P., S.S., S.A., P.G., N.M.C., K.P.A. and Á.R.-V.; Writing—review & editing, N.D., R.P., S.S., S.A., P.G. and K.P.A.; Visualization, N.D., R.P., S.A., P.G., N.M.C. and K.P.A.; Supervision, R.P. and S.A.; Project administration, N.D. and S.A.; Funding acquisition, S.A. and Á.R.-V. All authors have read and agreed to the published version of the manuscript.

Funding: The author thanks Vicerrectoria de Investigacion y Desarrollo (VRID) y Direccion de Investigacion y Creacion Artistica DICA, Proyecto presentado al Concurso VRID-Iniciación 2022, VRID N°2022000449-INI, Universidad de Concepción, Concepción, Chile. Centro Nacional de Excelencia para la Industria de la Madera (ANID BASAL FB210015 CENAMAD), Pontificia Universidad Católica de Chile, Vicuña Mackenna 7860, Santiago, Chile, and Dirección de Investigación de la Universidad Católica de la Santísima Concepción, Concepción, Chile.

Institutional Review Board Statement: Not applicable.

Informed Consent Statement: Not applicable.

Data Availability Statement: Not applicable.

Acknowledgments: The authors gratefully appreciate the support given by the Department of Civil Engineering, Alagappa Chettiar Government College of Engineering and Technology, Sivagangai, India, through the TEQIP-3 Project. The author thanks Vicerrectoria de Investigacion y Desarrollo (VRID) and Direccion de Investigacion y Creacion Artistica DICA, Proyecto presentado al Concurso VRID-Iniciación 2022, VRID N°2022000449-INI, Universidad de Concepción, Concepción, Chile. Centro Nacional de Excelencia para la Industria de la Madera (ANID BASAL FB210015 CENAMAD), Pontificia Universidad Católica de Chile, Vicuña Mackenna 7860, Santiago, Chile and Dirección de Investigación de la Universidad Católica de la Santísima Concepción, Concepción, Chile.

Conflicts of Interest: The authors declare no conflict of interest.

References

1. Ding, W.; Jia, S. An Improved Equation for the Bearing Capacity of Concrete-Filled Steel Tube Concrete Short Columns Based on GPR. *Buildings* **2023**, *13*, 1226. [CrossRef]
2. Emperger, F.V. *Welche Statische Bedeutung Hat Die Einbetonierungeiner Eisensaule*; Beton Eisen: Berlin, Germay, 1907; pp. 172–174.
3. Burr, W.H. The reinforced concrete work of the McGraw Building. *Trans. Am. Soc. Civ. Eng.* **1908**, *60*, 443–457. [CrossRef]
4. Yee, K.M.; Shakir-Khalil, H.; Taylor, R. Design expressions for a new type of composite column. *J. Constr. Steel Res.* **1982**, *2*, 26–32. [CrossRef]
5. Weng, C.C.; Yen, S.I. Comparisons of concrete-encased composite column strength provisions of ACI Code and AISC specification. *Eng. Struct.* **2002**, *24*, 59–72. [CrossRef]
6. Eom, T.-S.; Yang, J.-M.; Kim, D.-K.; Lim, J.-J.; Lee, S.-H. Experimental investigation of bolted end-plate angle splice in encased composite columns. *Eng. Struct.* **2019**, *190*, 31–40. [CrossRef]
7. Lai, B.; Liew, J.Y.R.; Hoang, A.L. Behavior of high strength concrete encased steel composite stub columns with C130 concrete and S690 Steel. *Eng. Struct.* **2019**, *200*, 109743. [CrossRef]
8. Khan, M.K.I.; Rana, M.M.; Zhang, Y.X.; Lee, C.K. Compressive behaviour of engineered cementitious composites and concrete encased steel composite columns. *J. Constr. Steel Res.* **2020**, *167*, 105967. [CrossRef]
9. AISC Frames and Other Structures. *Specification for Structural Steel Buildings (Allowable Stress Design and Plastic Design)*; American Institute of Steel Construction: Chicago, IL, USA, 1989; pp. 136–138.
10. *ANSI/AISC 360-16*; AISC Specification for Structural Steel Buildings. American Institute of Steel Construction: Chicago, IL, USA, 2010; p. 676.
11. Soman, M.; Mohan, J. Rehabilitation of RC columns using Ferrocement jacketing. *Constr. Build. Mater.* **2018**, *181*, 156–162. [CrossRef]
12. Campian, C.; Nagy, Z.; Pop, M. Behavior of fully encased steel-concrete composite columns subjected to monotonic and cyclic loading. *Procedia Eng.* **2015**, *117*, 439–451. [CrossRef]
13. Raju, S.; Rathinam, J.; Dharmar, B.; Rekha, S.; Avudaiappan, S.; Amran, M.; Usanova, K.I.; Fediuk, R.; Guindos, P.; Ramamoorthy, R.V. Cyclically Loaded Copper Slag Admixed Reinforced Concrete Beams with Cement Partially Replaced with Fly Ash. *Materials* **2022**, *15*, 3101. [CrossRef]
14. Giménez, E.; Adam, J.M.; Ivorra, S.; Calderón, P.A. Influence of strips configuration on the behaviour of axially loaded RC columns strengthened by steel angles and strips. *Mater. Des.* **2009**, *30*, 4103–4111. [CrossRef]
15. Hosseini Hashemi, B.; Jafari, M.A. Experimental Evaluation of Elastic Critical Load in Batten columns. *J. Constr. Steel Res.* **2009**, *65*, 125–131. [CrossRef]
16. Lee, K.; Bruneau, M. Seismic vulnerability evaluation of axially loaded steel built-uplaced members I: Experimental results. *Earthq. Eng. Eng. Vib.* **2008**, *7*, 113–124. [CrossRef]
17. Dar, M.A.; Sahoo, D.R.; Pulikkal, S.; Jain, A.K. Behaviour of laced built-up cold-formed steel columns: Experimental Investigation and Numerical Validation. *Thin-Walled Struct.* **2018**, *132*, 398–409. [CrossRef]
18. Wasserman, R.; Bentur, A. Interfacial interactions in lightweight aggregate concretes and their influence on the concrete strength. *Cem. Concr. Compos.* **1996**, *18*, 67–76. [CrossRef]
19. Wasserman, R.; Bentur, A. Effect of lightweight fly ash aggregate microstructure on the strength of concretes. *Cem. Concr. Res.* **1997**, *27*, 525–537. [CrossRef]
20. Jayanthi, V.; Avudaiappan, S.; Amran, M.; Arunachalam, K.P.; Qader, D.N.; Delgado, M.C.; Flores, E.I.S.; Rashid, R.S. Innovative use of micronized biomass silica-GGBS as agro-industrial by-products for the production of a sustainable high-strength geopolymer concrete. *Case Stud. Constr. Mater.* **2022**, *18*, e01782. [CrossRef]
21. Semenov, P.A.; Uzunian, A.V.; Davidenko, A.M.; Derevschikov, A.A.; Goncharenko, Y.M.; Kachanov, V.A.; Khodyrev, V.Y.; Meschanin, A.P.; Minaev, N.G.; Mochalov, V.V.; et al. First Study of radiation hardness of lead tungstate crystals at low temperatures. *Nucl. Instrum. Methods Phys. Res. Sect. A Accel. Spectrometers Detect. Assoc. Equip.* **2007**, *582*, 575–580. [CrossRef]
22. Tangtermsirikul, S.; Wijeyewickrema, A.C. Strength evaluation of aggregate made from fly ash. *ScienceAsia* **2000**, *26*, 237. [CrossRef]
23. Sheeba, K.R.J.; Priya, R.K.; Arunachalam, K.P.; Avudaiappan, S.; Maureira-Carsalade, N.; Roco-Videla, Á. Characterisation of Sodium Acetate Treatment on Acacia pennata Natural Fibres. *Polymers* **2023**, *15*, 1996. [CrossRef]

24. Haque, M.N.; Al-Khaiat, H.; Kayali, O. Strength and durability of lightweight concrete. *Cem. Concr. Compos.* **2004**, *26*, 307–314. [CrossRef]
25. Rohman, R.K.; Aji, S. Effect of fly ash on compressive strength of concrete containing recycled coarse aggregate. *AIP Conf. Proc.* **2018**, *2014*, 020097. [CrossRef]
26. Güneyisi, E.; Gesoğlu, M.; Pürsünlü, Ö.; Mermerdaş, K. Durability aspect of concretes composed of cold bonded and sintered fly ash lightweight aggregates. *Compos. Part B Eng.* **2013**, *53*, 258–266. [CrossRef]
27. Kayali, O. Fly ash lightweight aggregates in high performance concrete. *Constr. Build. Mater.* **2008**, *22*, 2393–2399. [CrossRef]
28. Kockal, N.U.; Ozturan, T. Effects of lightweight fly ash aggregate properties on the behavior of lightweight concretes. *J. Hazard. Mater.* **2010**, *179*, 954–965. [CrossRef]
29. Gomathi, P.; Sivakumar, A. Accelerated curing effects on the mechanical performance of cold bonded and sintered fly ash aggregate concrete. *Constr. Build. Mater.* **2015**, *77*, 276–287. [CrossRef]
30. Arunachalam, K.P.; Avudaiappan, S.; Flores, E.I.S.; Parra, P.F. Experimental Study on the Mechanical Properties and Microstructures of Cenosphere Concrete. *Materials* **2023**, *16*, 3518. [CrossRef] [PubMed]
31. Divyah, N.; Thenmozhi, R.; Neelamegam, M. Experimental and numerical analysis of battened built-up lightweight concrete encased composite columns subjected to axial cyclic loading. *Lat. Am. J. Solids Struct.* **2020**, *17*, e259. [CrossRef]
32. Jiang, C.; Fan, K.; Wu, F.; Chen, D. Experimental study on the mechanical properties and microstructure of chopped basalt fibre reinforced concrete. *Mater. Des.* **2014**, *58*, 187–193. [CrossRef]
33. Qin, J.; Qian, J.; Li, Z.; You, C.; Dai, X.; Yue, Y.; Fan, Y. Mechanical properties of basalt fiber reinforced magnesium phosphate cement composites. *Constr. Build. Mater.* **2018**, *188*, 946–955. [CrossRef]
34. Kharun, M.; Koroteev, D.D.; Dkhar, P.; Zdero, S.; Elroba, S.M. Physical and mechanical properties of basalt-fibered high-strength concrete. *Struct. Mech. Eng. Constr. Build.* **2018**, *14*, 396–403. [CrossRef]
35. Galishnikova, V.V.; Chiadighikaobi, P.C.; Emiri, D.A. Comprehensive view on the ductility of basalt fiber reinforced concrete focus on lightweight expanded clay. *Struct. Mech. Eng. Constr. Build.* **2019**, *15*, 360–366. [CrossRef]
36. Han, L.; Ren, Q.; Li, W. Inclined, tapered and STS concrete-filled steel tubular (CFST) stub columns under axial compression. In *Tubular Structures XIII, Proceedings of the 13th International Symposium on Tubular Structures, Hong Kong, China, 15–17 December 2010*; CRC Press: Boca Raton, FL, USA, 2010; pp. 623–628. [CrossRef]
37. Zhang, Y.; Liu, Y.; Xin, H.; He, J. Numerical parametric study on ultimate load and ductility of concrete encased equal-leg angle steel composite columns. *Eng. Struct.* **2019**, *200*, 109679. [CrossRef]
38. Baláž, I.J.; Koleková, Y.P.; Moroczová, L.O. Behaviour of steel laced built-up columns. In *Advances and Trends in Engineering Sciences and Technologies III*; CRC Press: Boca Raton, FL, USA, 2019; pp. 29–35. [CrossRef]
39. *IS 801-1975*; Practice for Use of Cold-Formed Light Gauge Steel Structural Members in General Building Construction. Bureau of Indian Standards: New Delhi, India, 1975.
40. Hosseini Hashemi, B.; Poursamad Bonab, A. Experimental investigation of the behavior of laced columns under constant axial load and cyclic lateral load. *Eng. Struct.* **2013**, *57*, 536–543. [CrossRef]
41. Tolstoy, A.; Lesovik, V.; Fediuk, R.; Amran, M.; Gunasekaran, M.; Vatin, N.; Vasilev, Y. Production of greener high-strength concrete using Russian quartz sandstone mine waste aggregates. *Materials* **2020**, *13*, 5575. [CrossRef] [PubMed]
42. Kim, C.-S.; Park, H.-G.; Chung, K.-S.; Choi, I.-R. Eccentric axial load testing for concrete-encased steel columns using 800 MPA Steel and 100 MPA concrete. *J. Struct. Eng.* **2012**, *138*, 1019–1031. [CrossRef]
43. Mazars, J.; Hamon, F.; Grange, S. A new 3D damage model for concrete under monotonic, cyclic and dynamic loadings. *Mater. Struct.* **2015**, *48*, 3779–3793. [CrossRef]
44. Di Re, P.; Addessi, D.; Filippou, F. Mixed 3D Beam Element with Damage Plasticity for the Analysis of RC Members under Warping Torsion. *J. Struct. Eng.* **2018**, *144*, 04018064. [CrossRef]
45. Yuan, F.; Wu, Y.-F. Effect of load cycling on plastic hinge length in RC Columns. *Eng. Struct.* **2017**, *147*, 90–102. [CrossRef]
46. Paul, M. Buckling loads for built-up columns with stay plates. *J. Eng. Mech.* **1995**, *121*, 1200–1208. [CrossRef]